

Inclusive production of Higgs boson in the two-photon channel at the LHC within k_t -factorization approach and with the standard model couplings

Antoni Szczurek,^{1,2,*} Marta Łuszczak,^{2,†} and Rafał Maciuła^{1,‡}

¹*Institute of Nuclear Physics PAN, PL-31-342 Kraków, Poland*

²*University of Rzeszów, PL-35-959 Rzeszów, Poland*

(Received 29 July 2014; revised manuscript received 3 October 2014; published 18 November 2014)

We calculate differential cross sections for the Higgs boson and/or two-photon production from the intermediate (virtual) Higgs boson within the formalism of k_t factorization. The off-shell $g^*g^* \rightarrow H$ matrix elements are used. We compare results obtained with infinite top fermion (quark) mass and with finite mass taken into account. The latter effect is rather small. We compare the results with different unintegrated gluon distributions from the literature. Two methods are used. In the first method first Higgs boson is produced in the $2 \rightarrow 1$ $gg \rightarrow H$ k_t -factorization approach and then isotropic decay with the Standard Model branching fraction is performed. In the second method we calculate directly two photons coupled to the virtual Higgs boson. The results of the two methods are compared and differences are discussed. The results for the two photons from the Higgs boson are compared with recent ATLAS Collaboration data. The leading-order $gg \rightarrow H$ contribution is rather small compared to the ATLAS experimental data ($\gamma\gamma$ transverse momentum and rapidity distributions) for all unintegrated gluon distributions from the literature. We include also the higher-order contribution $gg \rightarrow H(\rightarrow \gamma\gamma)g$, $gg \rightarrow gHg$ and the contribution of the W^+W^- and Z^0Z^0 . The $gg \rightarrow Hg$ mechanism gives a similar cross section as the $gg \rightarrow H$ mechanism. We argue that there is almost no double counting when adding $gg \rightarrow H$ and $gg \rightarrow Hg$ contributions due to the different topology of Feynman diagrams. The final sum is comparable with the ATLAS two-photon data. We discuss uncertainties related to both the theoretical approach and existing unintegrated gluon distribution functions.

DOI: [10.1103/PhysRevD.90.094023](https://doi.org/10.1103/PhysRevD.90.094023)

PACS numbers: 12.38.Bx, 14.80.Bn, 14.70.Bh, 13.85.Qk

I. INTRODUCTION

The Higgs-like boson has been discovered recently at the LHC [1]. It has been observed in a few decay channels. The $\gamma\gamma$ and Z^0Z^0 are particularly spectacular [2–5]. Before the discovery many of the Higgs properties were strongly dependent on its mass. Now knowing the Higgs boson mass $M_H \approx 126$ GeV we can fix the parameters for production and decay of the Higgs boson, at least within the Standard Model. We slowly enter an era of more detailed studies. In particular, it is very important to know what is the Higgs boson spin and parity and if it is a Standard Model object. Also understanding the rapidity and transverse momentum distributions is particularly interesting. While the total cross section is well under control and was calculated in leading-order (LO), next-to-leading-order (NLO) and even next-to-next-to-leading-order (NNLO) approximation [6] the distribution in the Higgs boson transverse momentum is more challenging. This can be addressed e.g. in the transverse momentum resummation approach (see e.g. Refs. [7,8] and references therein).

It was advocated recently that precise differential data for the Higgs boson in the two-photon final channel could be very useful to test and explore unintegrated gluon distribution

functions (UGDFs) [9]. It was shown very recently [10] that the k_t -factorization formalism with commonly used UGDFs [Kimber-Martin-Ryskin (KMR) [11] and Jung Catani-Ciafaloni-Fiorani-Marchesini (CCFM) [12]] gives a reasonable description of recent ATLAS data obtained at $\sqrt{s} = 8$ TeV [14]. We perform a similar calculation and, as will be seen in the following, draw slightly different conclusions.

In the present study we present several differential distributions for the Higgs boson and photons from the Higgs boson decay at $\sqrt{s} = 8$ TeV for various UGDFs from the literature [11–13], also the ones used in the context of low- x physics (Kutak-Staśto [15] and Kutak-Sapeta [16]). We include both leading-order and next-to-leading-order contributions. We shall critically discuss uncertainties and open problems in view of the recent ATLAS data.

II. FORMALISM

A. Higgs boson production

In the k_t -factorization approach [17,18] the cross section for the Higgs boson production can be written somewhat formally as

$$\begin{aligned} \sigma_{pp \rightarrow H} = & \int \frac{dx_1}{x_1} \frac{dx_2}{x_2} \frac{d^2q_{1t}}{\pi} \frac{d^2q_{2t}}{\pi} \delta((q_1 + q_2)^2 - M_H^2) \sigma_{gg \rightarrow H} \\ & \times (x_1, x_2, q_1, q_2) \\ & \times \mathcal{F}_g(x_1, q_{1t}^2, \mu_F^2) \mathcal{F}_g(x_2, q_{2t}^2, \mu_F^2), \end{aligned} \quad (2.1)$$

*antoni.szczurek@ifj.edu.pl

†luszczak@univ.rzeszow.pl

‡rafal.maciula@ifj.edu.pl

where \mathcal{F}_g are so-called unintegrated (or transverse-momentum-dependent) gluon distributions and $\sigma_{gg \rightarrow H}$ is the $gg \rightarrow H$ (off-shell) cross section. The situation is illustrated diagrammatically in Fig. 1.

It is easy to show in the collinear approximation (see e.g. Ref. [19]) that

$$\sigma_{gg \rightarrow H} = \frac{\pi}{\hat{s}} \delta(\hat{s} - m_H^2). \quad (2.2)$$

After some manipulation the formula (2.1) can be written conveniently as (see Ref. [20])

$$\begin{aligned} \sigma_{pp \rightarrow H} = & \int dy d^2 p_t d^2 q_t \frac{1}{sx_1 x_2} \frac{1}{m_{t,H}^2} |\mathcal{M}_{g^* g^* \rightarrow H}|^2 \\ & \times \mathcal{F}_g(x_1, q_{1t}^2, \mu_F^2) \mathcal{F}_g(x_2, q_{2t}^2, \mu_F^2) / 4, \end{aligned} \quad (2.3)$$

which can be also used to calculate the rapidity and transverse momentum distribution of the Higgs boson.

In the last equation, $\vec{p}_t = \vec{q}_{1t} + \vec{q}_{2t}$ is the transverse momentum of the Higgs boson and $\vec{q}_t = \vec{q}_{1t} - \vec{q}_{2t}$ is the auxiliary variable which is used in the integration. Furthermore, $m_{t,H}$ is the so-called Higgs transverse mass and $x_1 = \frac{m_{t,H}}{\sqrt{s}} \exp(y)$, $x_2 = \frac{m_{t,H}}{\sqrt{s}} \exp(-y)$. The factor $\frac{1}{4}$ is the Jacobian of transformation from $(\vec{q}_{1t}, \vec{q}_{2t})$ to (\vec{p}_t, \vec{q}_t) variables.

Similar formalism was used in the past for the production of gauge bosons [22]. There gluon distributions have to be replaced by unintegrated quark and antiquark distributions.

Let us concentrate for a while on the matrix element for the $g^* g^* \rightarrow H$. In Ref. [20] the on-shell matrix element was used. In Ref. [23] the off-shell matrix element was used instead, however in the approximation of an infinitely heavy top in the triangle coupling of gluons to the Higgs boson (see also [21] where the off-shell matrix element was discussed). Then the effective $g^* g^* \rightarrow H$ coupling is relatively simple. The matrix element under discussion (for the on-shell Higgs boson) takes the simple form:

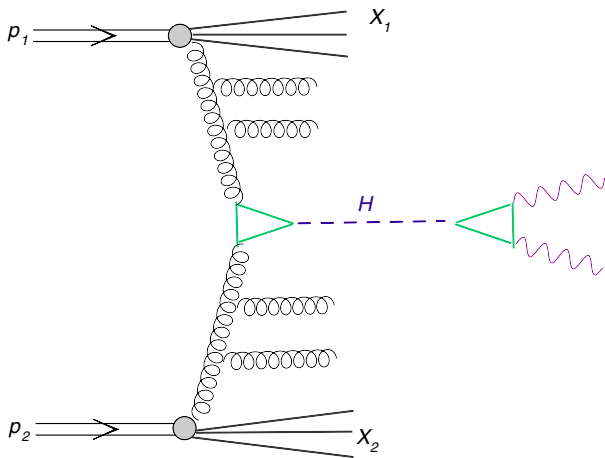


FIG. 1 (color online). Dominant leading-order diagram for inclusive Higgs boson production in the two-photon channel.

$$\mathcal{M}_{g^* g^* \rightarrow H} = -i \delta^{ab} \frac{\alpha_s}{4\pi v} (m_H^2 + p_t^2) \cos(\phi) \frac{2}{3}, \quad (2.4)$$

where $v^2 = (G_F \sqrt{2})^{-1}$. The effect of finite-mass corrections was studied in Ref. [24] in the context of k_t factorization and in [25] in the context of higher-order collinear approximation corrections. Then the corresponding matrix element is more complicated and can be written with the help of two form factors:

$$\begin{aligned} \mathcal{M}_{g^* g^* \rightarrow H} = & -i \delta^{ab} \frac{\alpha_s}{4\pi v} \left[(m_H^2 + p_t^2) \cos(\phi) G_1(q_1, q_2, q) \right. \\ & \left. - \frac{2(m_H^2 + p_t^2)^2 |q_{1t}| |q_{2t}|}{(m_H^2 + q_{1t}^2 + q_{2t}^2)} G_2(q_1, q_2, q) \right]. \end{aligned} \quad (2.5)$$

The form factors G_1 and G_2 have an integral representation. However, at not too big virtualities of gluons and the Higgs boson the following approximate formula for the G_1 and G_2 form factors can be used [24]:

$$G_1 = \frac{2}{3} \left(1 + \frac{7}{30} \chi + \frac{2}{21} \chi^2 + \frac{11}{30} (\xi_1 + \xi_2) + \dots \right), \quad (2.6)$$

$$G_2 = -\frac{1}{45} (\chi - \xi_1 - \xi_2) - \frac{4}{315} \chi^2 + \dots, \quad (2.7)$$

where the expansion variables χ , ξ_1 , ξ_2 above are defined as

$$\chi = \frac{q^2}{4m_f^2}, \quad (2.8)$$

$$\xi_1 = \frac{q_1^2}{4m_f^2} < 0, \quad (2.9)$$

$$\xi_2 = \frac{q_2^2}{4m_f^2} < 0. \quad (2.10)$$

B. $H \rightarrow \gamma\gamma$

The matrix element for the Higgs boson decay into photons with helicity λ_1 and λ_2 can be written as

$$\mathcal{M}_{H \rightarrow \gamma\gamma}(\lambda_1, \lambda_2) = T_{H \rightarrow \gamma\gamma}^{\mu\nu} \epsilon_\mu^*(\lambda_1) \epsilon_\nu^*(\lambda_2). \quad (2.11)$$

The LO vertex function can be decomposed as the sum

$$T_{H \rightarrow \gamma\gamma}^{\mu\nu} = T_{H \rightarrow \gamma\gamma}^{\mu\nu, W} + T_{H \rightarrow \gamma\gamma}^{\mu\nu, t} + \dots, \quad (2.12)$$

where the first term includes loops with intermediate W^\pm and the second term triangle(s) with top quarks. The dots represent the contribution of triangles with bottom and charm quarks and with τ leptons, etc. The vertex function can be written as

$$T_{H \rightarrow \gamma\gamma}^{\mu\nu}(p_1, p_2) = i \frac{\alpha_{\text{em}}}{2\pi} \mathcal{A}(G_F \sqrt{2})^{1/2} (p_2^\mu p_1^\nu - (p_1 \cdot p_2) g^{\mu\nu}). \quad (2.13)$$

In the Standard Model the \mathcal{A} constant is

$$\mathcal{A} = \mathcal{A}_W(\tau_W) + N_c e_f^2 \mathcal{A}_f(\tau_f) + \dots, \quad (2.14)$$

where the arguments are

$$\tau_W = \frac{m_H^2}{4m_W^2}, \quad \tau_f = \frac{m_H^2}{4m_f^2}. \quad (2.15)$$

The functions \mathcal{A}_W and \mathcal{A}_f have the simple form:

$$\mathcal{A}_W(\tau) = -(2\tau^2 + 3\tau + 3(2\tau - 1)f(\tau))/\tau^2, \quad (2.16)$$

$$\mathcal{A}_f(\tau) = 2(\tau + (\tau - 1)f(\tau))/\tau^2, \quad (2.17)$$

where the function $f(\tau)$ reads

$$f(\tau) = \arcsin^2(\sqrt{t}). \quad (2.18)$$

For light fermions the function $f(\tau)$ is slightly different [26].

The two-photon decay width can be calculated as

$$\Gamma_{H \rightarrow \gamma\gamma} = \frac{1}{32\pi^2} \sum_{\lambda_1, \lambda_2} |\mathcal{M}_{H \rightarrow \gamma\gamma}(\lambda_1, \lambda_2)|^2 \frac{p}{m_H^2} \frac{1}{2}. \quad (2.19)$$

The factor $\frac{1}{2}$ is due to the identity of the final state photons. Using Eq. (2.19) with the matrix element given by Eq. (2.11) we get $\Gamma_{H \rightarrow \gamma\gamma} = 0.91 \times 10^{-5}$ which, when combined with the total decay width $\Gamma_H \approx 4$ MeV [27], gives the branching fraction $\text{BF}_{H \rightarrow \gamma\gamma} = 2.27 \times 10^{-5}$, consistent with what is known from the literature (see e.g. Ref. [28]). Two-loop corrections are rather very small [29].

C. $g^* g^* \rightarrow H^* \rightarrow \gamma\gamma$

Let us combine now all elements defined above and write the matrix element for the $g^* g^* \rightarrow H^* \rightarrow \gamma\gamma$ process,

$$\begin{aligned} \mathcal{M}_{g^* g^* \rightarrow H^* \rightarrow \gamma\gamma}(\lambda_1, \lambda_2) &= \mathcal{M}_{g^* g^* \rightarrow H^*}(\vec{q}_{1t}, \vec{q}_{2t}; \hat{s}) \\ &\times \frac{1}{\hat{s} - M_H^2 + i\Gamma_H M_H} \mathcal{M}_{H^* \rightarrow \gamma\gamma}(\lambda_1, \lambda_2). \end{aligned} \quad (2.20)$$

In the infinitely heavy quark approximation the matrix element squared averaged over colors can be written in the quite compact way (see Ref. [10]):

$$\begin{aligned} \frac{d\sigma}{dy_H dy_p d^2 p_t}(y_H, y_p, p_t) &= \frac{1}{16\pi^2 \hat{s}^2} \times \left\{ x_1 g_1(x_1, \mu^2) x_2 g_2(x_2, \mu^2) \overline{|\mathcal{M}_{gg \rightarrow Hg}|^2} + \left[\sum_{f_1=-3,3} x_1 q_{1,f_1}(x_1, \mu^2) \right] x_2 g_2(x_2, \mu^2) \overline{|\mathcal{M}_{qg \rightarrow Hq}|^2} \right. \\ &\quad \left. + x_1 g_1(x_1, \mu^2) \left[\sum_{f_2=-3,3} x_2 q_{2,f_2}(x_2, \mu^2) \right] \overline{|\mathcal{M}_{gq \rightarrow Hq}|^2} + \sum_{f=-3,3} x_1 q_{1,f}(x_1, \mu^2) x_2 q_{2,-f}(x_2, \mu^2) \overline{|\mathcal{M}_{qq \rightarrow Hq}|^2} \right\}. \end{aligned} \quad (2.23)$$

$$\overline{|\mathcal{M}|^2} = \frac{1}{1152\pi^4} \alpha_{em}^2 \alpha_s^2 G_F^2 |\mathcal{A}|^2 \frac{\hat{s}^2 (\hat{s} + p_t^2)^2}{(\hat{s} - m_H^2)^2 + m_H^2 \Gamma_H^2} \cos^2(\phi). \quad (2.21)$$

The differential (in photon rapidities y_1, y_2 and transverse momenta p_{1t}, p_{2t}) cross section for the production of a pair of photons from the $g^* g^* \rightarrow H^* \rightarrow \gamma\gamma$ subprocess with an intermediate virtual Higgs boson can be written as

$$\begin{aligned} \frac{d\sigma(pp \rightarrow HX \rightarrow \gamma\gamma X)}{dy_1 dy_2 d^2 p_{1t} d^2 p_{2t}} &= \frac{1}{16\pi^2 \hat{s}^2} \cdot \frac{1}{2} \cdot \int \frac{d^2 k_{1t}}{\pi} \frac{d^2 k_{2t}}{\pi} \overline{|\mathcal{M}_{g^* g^* \rightarrow H^* \rightarrow \gamma\gamma}^{\text{off}}|^2} \\ &\times \delta^2(\vec{k}_{1t} + \vec{k}_{2t} - \vec{p}_{1t} - \vec{p}_{2t}) \\ &\times \mathcal{F}_g(x_1, k_{1t}^2, \mu^2) \mathcal{F}_g(x_2, k_{2t}^2, \mu^2). \end{aligned} \quad (2.22)$$

Please note that in this case the $m_H^2 + p_t^2$ term in Eq. (2.4) for the on-shell Higgs boson is replaced by $\hat{s} + p_t^2$ for the virtual Higgs boson. This has consequences some distance from the resonance position where the cross section is however small. In principle, also M_H^2 in the definition of the \mathcal{A} functions should be replaced by \hat{s} here.

Since we integrate over full phase space in y_1, y_2, p_{1t} and p_{2t} we have to include in addition an identity factor $\frac{1}{2}$, in full analogy to the calculation of the decay width into two photons.

How to remove the δ function in Eq. (2.22) in a convenient way for calculation is described in Ref. [30]. The calculation of the cross section according to formula (2.22) with matrix element (2.21) is not easy as the light Higgs boson discovered recently is a very narrow resonance. This calculation is performed within a Monte Carlo method using a well-known package VEGAS [31]. We have carefully tested both numerics and convergence.

D. $gg \rightarrow Hg$

In the collinear approximation the cross section for fixed-order processes of the type $p_1 p_2 \rightarrow H p_3$ (parton1 + parton2 \rightarrow Higgs + parton3) (see Fig. 2) of the order of α_s has been well known for a long time [32].

The corresponding cross section differential in Higgs boson rapidity (y_H), associated parton rapidity (y_p) and transverse momentum of each of them can be written as

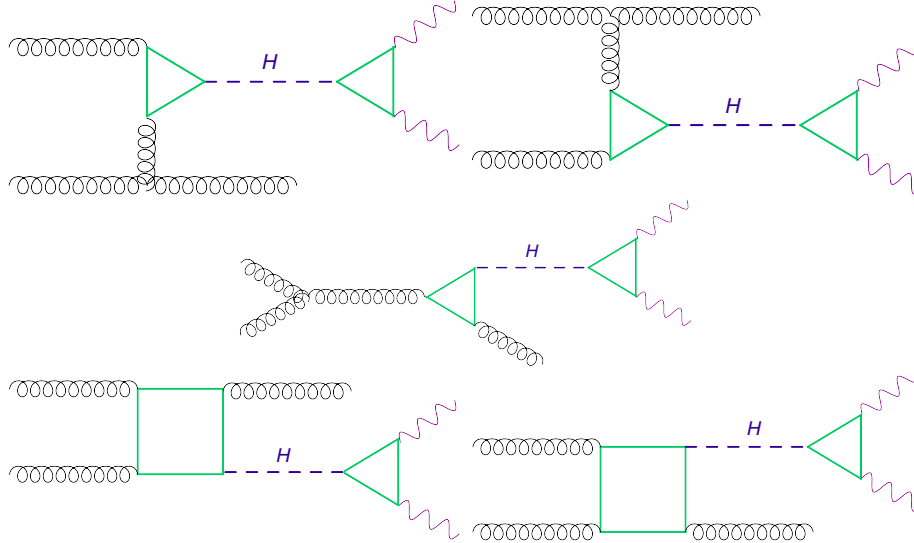


FIG. 2 (color online). Typical diagrams for QCD NLO contributions to the Higgs boson production.

The indices f in the formula above number both quarks ($f > 0$) and antiquarks ($f < 0$). Only three light flavors are included in actual calculations here. The explicit formulas for $|\overline{\mathcal{M}}|^2$ can be found in Ref. [32]. We have checked that the $gg \rightarrow Hg$ contribution dominates over the two other types of contributions. This can be understood as due to the presence of the box contributions for $gg \rightarrow Hg$ but is absent in the other cases.

In the following we shall calculate the dominant $gg \rightarrow Hg$ contribution also taking into account the transverse momenta of the initial gluons. In the k_t factorization the NLO differential cross section can be written as

$$\begin{aligned} \frac{d\sigma(pp \rightarrow HgX)}{dy_H dy_g d^2 p_{H,t} d^2 p_{g,t}} &= \frac{1}{16\pi^2 \hat{s}^2} \int \frac{d^2 q_{1t}}{\pi} \frac{d^2 q_{2t}}{\pi} \overline{|\mathcal{M}_{g^*g^* \rightarrow Hg}^{\text{off-shell}}|^2} \\ &\times \delta^2(\vec{q}_{1t} + \vec{q}_{2t} - \vec{p}_{H,t} - \vec{p}_{g,t}) \\ &\times \mathcal{F}(x_1, q_{1t}^2, \mu^2) \mathcal{F}(x_2, q_{2t}^2, \mu^2). \end{aligned} \quad (2.24)$$

This can be further simplified as discussed e.g. in Ref. [30].

Calculation of the off-shell matrix element for the process under consideration is rather complicated in the most general case as it involves loops (triangles and boxes). Since the box diagrams with very heavy top quarks/antiquarks dominate at high energies we expect that the off-shell effects should be relatively small. In the present approach we make the following replacement to simplify the calculation:

$$\overline{|\mathcal{M}_{g^*g^* \rightarrow Hg}^{\text{off-shell}}|^2} \rightarrow \overline{|\mathcal{M}_{gg \rightarrow Hg}^{\text{on-shell}}(s, t, u)|^2}, \quad (2.25)$$

where the latter is an analytical continuation of the on-shell matrix element off mass shell. The larger q_{1t} or q_{2t} the worse the approximation could be. This cannot be quantified, however, before the exact off-shell matrix element is calculated. This goes beyond the scope of the present study.

E. Higgs boson and dijets in the context of the k_t -factorization approach

It is well known that in contrast to gauge boson (W^\pm and Z^0) production for calculating the inclusive cross section for the Higgs boson production not only LO but also NLO and even NNLO corrections are pretty large. Collinear NNLO contributions to the Higgs boson production associated with dijet production was discussed e.g. in Ref. [38]. A somewhat simplified but pedagogical high-energy approach was discussed in Ref. [39].

In the present analysis we wish to make a reference to the $gg \rightarrow H$ k_t -factorization calculations so a simplified approach may be useful. In the following we shall evaluate the cross section and differential distributions in the collinear approximation for the subprocesses shown in Fig. 3. At large q_{1t} and q_{2t} [transverse momenta of the exchanged (red online) gluons] the contribution of the first subprocess ($gg \rightarrow gHg$) can be directly compared to the k_t -factorization result with the KMR UGDF. This may be useful in order to understand higher-order contributions contained in the k_t -factorization approach.

The matrix element for the $gg \rightarrow gHg$ which can (should) be used to compare the collinear-factorization result with the k_t -factorization approach result reads

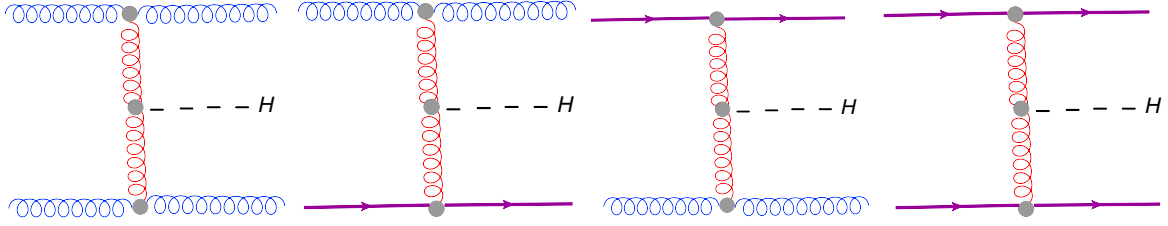


FIG. 3 (color online). The $2 \rightarrow 3$ diagrams which are used in order to make reference to the $2 \rightarrow 1$ k_T -factorization calculation.

$$\begin{aligned}
 \mathcal{M}_{\lambda_1 \lambda_2 \rightarrow \lambda_3 \lambda_4}^{gg \rightarrow gHg} (ace, bde') & \\
 &= g_s(\mu_{r,1}^2) f_{ace} \epsilon_{\mu_1}(\lambda_1) C^{\mu_1 \nu_1 \tau_1}(-p_1, p_3, q_1) \epsilon_{\nu_1}^*(\lambda_3) \\
 &\times \frac{(-ig_{\tau_1 \tau_1'})}{t_1} T_{gg \rightarrow H}^{\tau_1' \tau_2'}(q_1, q_2, p_H) \frac{(-ig_{\tau_2 \tau_2'})}{t_2} \\
 &\times g_s(\mu_{r,2}^2) f_{bde'} \epsilon_{\mu_2}(\lambda_2) C^{\mu_2 \nu_2 \tau_2}(-p_2, p_4, q_2) \epsilon_{\nu_2}^*(\lambda_4), \quad (2.26)
 \end{aligned}$$

where dependence on the renormalization scale was made explicit.

Here the matrix element is evaluated as in Ref. [39] using high-energy approximations. It can be written somewhat schematically as

$$\begin{aligned}
 |\overline{\mathcal{M}}_{gg \rightarrow gHg}|^2 &= 4 \frac{C_A^2}{N_c^2 - 1} g_s^2(\mu_{r,1}^2) g_s^2(\mu_{r,2}^2) \\
 &\times \frac{\hat{s}}{t_1^2 t_2^2} |C_{gg \rightarrow H}(q_1, p_H, q_2)|^2. \quad (2.27)
 \end{aligned}$$

The matrix element is particularly simple in the limit:

$$s_{ij} \gg s_{iH}, \quad s_{jH} \gg m_H^2. \quad (2.28)$$

We have made explicit running of a strong coupling constant in (2.27). In practical calculation it is reasonable to take $\mu_{r,1}^2 = p_{3t}^2$ and $\mu_{r,2}^2 = p_{4t}^2$. At high energies $t_1 \approx -q_{1t}^2 = -p_{3t}^2$ and $t_2 \approx -q_{2t}^2 = -p_{4t}^2$.

The phase space integration is performed then with the $gg \rightarrow gHg$ matrix element squared and collinear gluon distribution functions (GDFs), see for example the next subsection. Both integrated and differential cross sections can be then compared with those obtained within the k_T -factorization approach. Especially inspiring is to understand the interrelation between the two approaches for larger jet/Higgs transverse momenta p_{3t}, p_{4t}, p_{tH} .

In the high-energy approach quark and antiquarks contributions can be easily included by replacing gluon distributions $g(x_1, \mu_{f,1}^2)$ and $g(x_2, \mu_{f,2}^2)$ by so-called effective parton distributions (see e.g. Ref. [40]):

$$\begin{aligned}
 f_{\text{eff}}(x_k, \mu_k^2) &= g(x_k, \mu_k^2) + \frac{C_F}{C_A} (u(x_k, \mu_k^2) + d(x_k, \mu_k^2) \\
 &+ s(x_k, \mu_k^2) + \bar{u}(x_k, \mu_k^2) + \bar{d}(x_k, \mu_k^2) \\
 &+ \bar{s}(x_k, \mu_k^2)). \quad (2.29)
 \end{aligned}$$

A similar procedure is often done in the context of Mueller-Navelet jets. We shall evaluate and show the quark/antiquark components separately as they are not taken into account explicitly in the k_T -factorization approach.

F. WW fusion

Now we wish to consider purely electroweak corrections that are known to give a sizeable contribution to the Higgs boson production.

The second most important mechanism for the Higgs boson production is the fusion of off-shell gauge bosons: WW or ZZ . It is known that at the LHC energy the WW fusion constitutes about 10%–15% of the integrated inclusive cross section. If the weak boson fusion contribution was separated, the measurement of the WWH (or ZZH) coupling would be a very interesting test of the Standard Model.

In the present paper we are interested in the differential distributions of the Higgs boson rather than in the integrated cross section.

For the gauge boson fusion the partonic subprocess is of the $2 \rightarrow 3$ type: $q(p_1) + q(p_2) \rightarrow q(p_3) + q(p_4) + H(p_H)$ (see Fig. 4).

The corresponding proton-proton cross section can be written as

$$\begin{aligned}
 d\sigma &= \mathcal{F}_{12}^{VV}(x_1, x_2) \frac{1}{2\hat{s}} |\overline{\mathcal{M}}_{qq \rightarrow qqH}|^2 \\
 &\times \frac{d^3 p_3}{(2\pi)^3 2E_3} \frac{d^3 p_4}{(2\pi)^3 2E_4} \frac{d^3 p_H}{(2\pi)^3 2E_H} \\
 &\times (2\pi)^4 \delta^4(p_1 + p_2 - p_3 - p_4 - p_H) dx_1 dx_2. \quad (2.30)
 \end{aligned}$$

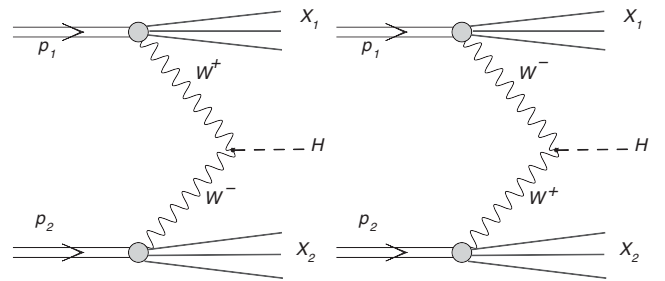


FIG. 4. Diagrams for the WW fusion.

The next-to-leading-order corrections to the matrix element of the WW fusion are rather small [33]. The leading-order subprocess matrix element was calculated first in Ref. [34]. The spin-averaged matrix element squared reads

$$\overline{|\mathcal{M}|^2} = 128\sqrt{2}G_F^3 \frac{M_W^8(p_1 \cdot p_2)(p_3 \cdot p_4)}{(2p_3 \cdot p_1 + M_W^2)^2(2p_4 \cdot p_2 + M_W^2)^2}. \quad (2.31)$$

For the WW fusion, limiting to light flavors, the partonic function is

$$\begin{aligned} \mathcal{F}_{12}^{WW}(x_1, x_2) = & (u_1(x_1, \mu_1^2) + \bar{d}_1(x_1, \mu_1^2) + \bar{s}_1(x_1, \mu_1^2)) \\ & \times (\bar{u}_2(x_2, \mu_2^2) + d_2(x_2, \mu_2^2) + s_2(x_2, \mu_2^2)) \\ & + (\bar{u}_1(x_1, \mu_1^2) + d_1(x_1, \mu_1^2) + s_1(x_1, \mu_1^2)) \\ & \times (u_2(x_2, \mu_2^2) + \bar{d}_2(x_2, \mu_2^2) + \bar{s}_2(x_2, \mu_2^2)). \end{aligned} \quad (2.32)$$

In the following we take $\mu_1^2 = \mu_2^2 = M_H^2$. It is convenient to introduce the following new variables:

$$\vec{p}_+ = \vec{p}_3 + \vec{p}_4, \quad \vec{p}_- = \vec{p}_3 - \vec{p}_4, \quad (2.33)$$

which allow us to eliminate the momentum-dependent $\delta^3(\dots)$ in Eq. (2.30). Instead of integrating over x_1 and x_2 we shall integrate over $y_1 \equiv \ln(1/x_1)$ and $y_2 \equiv \ln(1/x_2)$.

$$\overline{|\mathcal{M}|_{f_1 f_2}^2} = 128\sqrt{2}G_F^3 M_Z^8 \frac{C_1^Z(f_1 f_2)(p_1 \cdot p_2)(p_3 \cdot p_4) + C_2^Z(f_1 f_2)(p_1 \cdot p_4)(p_2 \cdot p_3)}{(2p_3 \cdot p_1 + M_Z^2)^2(2p_4 \cdot p_2 + M_Z^2)^2}. \quad (2.35)$$

The flavor-dependent coefficients read

$$\begin{aligned} C_1^Z(f_1 f_2) = & \frac{1}{4}((V_{f_1} - A_{f_1})^2(V_{f_2} - A_{f_2})^2 \\ & + (V_{f_1} + A_{f_1})^2(V_{f_2} + A_{f_2})^2), \\ C_2^Z(f_1 f_2) = & \frac{1}{4}((V_{f_1} - A_{f_1})^2(V_{f_2} + A_{f_2})^2 \\ & + (V_{f_1} + A_{f_1})^2(V_{f_2} - A_{f_2})^2). \end{aligned} \quad (2.36)$$

The V_f and A_f are well-known vector and axial-vector couplings of the Z^0 boson to quarks/antiquarks. They can be expressed in terms of a third component of the weak isospin, charge of quark/antiquark and sinus of the Weinberg angle.

The differential cross section is calculated in exactly the same way as for the WW fusion.

H. Associated production with W and Z bosons

For completeness one could include also production of the Higgs boson associated with gauge bosons W^+ , W^- and Z^0 . These are formally lower-order ($2 \rightarrow 2$) processes than

Then using Eq. (2.30) we can write the inclusive spectrum of the Higgs boson as

$$\begin{aligned} \frac{d\sigma}{dyd^2p_t} = & \int dy_1 dy_2 x_1 x_2 \mathcal{F}(x_1, x_2, \mu_1^2, \mu_2^2) \\ & \times \frac{1}{2\hat{s}} \frac{d^3p_-}{16} \overline{|\mathcal{M}_{qq \rightarrow qqH}|^2} \frac{1}{2E_3} \frac{1}{2E_4} \\ & \times \frac{1}{(2\pi)^5} \delta(E_1 + E_2 - E_3 - E_4 - E_H). \end{aligned} \quad (2.34)$$

This is effectively a four-dimensional integral which can be calculated numerically.

Strong and electroweak corrections to the Higgs boson production via vector-boson fusion at the LHC were calculated e.g. in Refs. [35,36]. The corrections are relatively small and in the following analysis we shall show only leading-order results as a reference to the k_T -factorization result.

G. ZZ fusion

The ZZ fusion (see Fig. 5) can be calculated in an analogous way.

The corresponding matrix element depends on the subprocess type (set of quark, antiquark flavors). It can be written as [34]

the WW and ZZ fusion ($2 \rightarrow 3$) processes considered above. They were first considered in Ref. [37].

The matrix elements are very simple:

$$\begin{aligned} |\mathcal{M}_{f_1 f_2 \rightarrow WH}|^2 = & \frac{(G_F M_W^2)^2}{72\pi^2} |V_{f_1 f_2}|^2 \frac{3M_W^2 + p_W^2}{(\hat{s} - M_W^2)^2}, \\ |\mathcal{M}_{ff \rightarrow ZH}|^2 = & \frac{(G_F M_Z^2)^2}{72\pi^2} (V_f^2 + A_f^2) \frac{3M_Z^2 + p_Z^2}{(\hat{s} - M_Z^2)^2}. \end{aligned} \quad (2.37)$$

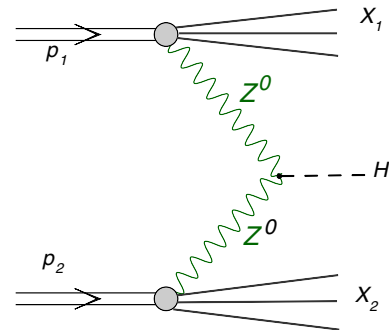


FIG. 5 (color online). Typical diagram for the ZZ fusion.

In the equation above p_V is the momentum of the gauge boson in the HV center-of-mass frame:

$$p_W^2 = \frac{1}{4\hat{s}}(\hat{s}^2 + M_V^4 + M_H^4 - 2\hat{s}M_V^2 - 2\hat{s}M_H^2 - 2M_V^2M_H^2), \quad (2.38)$$

where $V = W, Z$.

The fully differential cross section can be written as

$$\begin{aligned} \frac{d\sigma}{dy_H dy_W d^2 p_t} &= \frac{1}{16\pi\hat{s}^2} |\mathcal{M}_{f_1 f_2 \rightarrow WH}|^2 \\ &\times \sum_{f_1 f_2} (x_1 q_{f_1}(x_1, \mu^2) x_2 \bar{q}_{f_2}(x_2, \mu^2) \\ &+ x_1 \bar{q}_{f_1}(x_1, \mu^2) x_2 q_{f_2}(x_2, \mu^2)), \\ \frac{d\sigma}{dy_H dy_Z d^2 p_t} &= \frac{1}{16\pi\hat{s}^2} |\mathcal{M}_{ff \rightarrow ZH}|^2 \\ &\times \sum_f (x_1 q_f(x_1, \mu^2) x_2 \bar{q}_f(x_2, \mu^2) \\ &+ x_1 \bar{q}_f(x_1, \mu^2) x_2 q_f(x_2, \mu^2)). \end{aligned} \quad (2.39)$$

The Higgs boson distributions can be obtained from those above by integrating over y_W and y_Z , respectively.

III. RESULTS

A. $gg \rightarrow H$ and subsequent $H \rightarrow \gamma\gamma$ decay

In Table I we present the total (integrated over full phase space) cross section for the $2 \rightarrow 1$ gluon-gluon fusion mechanism for several UGDFs from the literature at $\sqrt{s} = 8$ TeV. For reference the leading-order collinear approximation result is typically 5–7 pb depending somewhat on the parton distribution functions used in the calculation. The k_t -factorization results (for several

UGDFs used here) are similar, except for the Kutak-Stasto and Kutak-Sapeta UGDFs which give much smaller numbers. There are two reasons for this. First, when calculating the gluon longitudinal momentum fractions the transverse momentum of the Higgs boson is included which increases x_1 and x_2 and therefore lowers the cross section. Secondly, many low- x UGDFs do not apply and/or are too small in the region of $x_1, x_2 > 0.01$. Quite different cross sections are obtained for different UGDFs. This shows that the UGDFs (often fitted only to HERA data) are much more uncertain than the collinear GDFs fitted to many sets of high-energy data. However, UGDFs have the advantage that they can be used for correct (exclusive) kinematics including transverse momenta of initial gluons, which cannot be addressed properly in collinear calculations.

For comparison in the middle block we show the contribution of $ij \rightarrow iHj$ processes calculated in the collinear-factorization approach for the jet transverse momenta bigger than 10 GeV. The $gg \rightarrow gHg$ contribution is of similar size as that for the leading-order $gg \rightarrow H$ k_t -factorization approach. We think that the latter contribution is to a large extent contained in the calculation with the KMR UGDF. However, the quark and antiquark initiated contributions which are also fairly large (~ 0.6 pb) must be included in addition explicitly.

At the very bottom we show contributions of the WW and ZZ fusions. The electroweak contribution is quite sizeable. As will be shown below they play an important role at large Higgs boson transverse momenta.

The so different cross sections obtained with different UGDFs may be partially understood by looking at the distribution in x_1 or x_2 (see Fig. 6). The KMR UGDF gives a much larger contribution in the region of $x_1, x_2 > 0.01$ than the typically small- x UGDFs. The other UGDFs are not very realistic in this range of x .

TABLE I. The cross section for Higgs production $p_t < 400$ GeV in pb for $\sqrt{s} = 8$ TeV and for different UGDFs from the literature. For comparison we show also the contribution of the $gg \rightarrow gHg$ and $ij \rightarrow iHj$ processes ($p_{1t}, p_{2t} > 10$ GeV), and WW and ZZ fusion.

Contribution	$\mu_r^2 = \mu_f^2 = m_H^2$
KMR	5.2349
Jung CCFM (set A0)	8.2705
Jung CCFM (set A+)	12.3791
Jung CCFM (set A-)	5.7335
Hautmann-Jung (set 2)	20.3774
Kutak-Stasto	2.6074
Kutak-Sapeta	1.5465
KMR, $q_{1t}, q_{2t} > 10$ GeV	2.4585
$gg \rightarrow gHg$, $q_{1t}, q_{2t} > 10$ GeV	0.24
$ij \rightarrow iHj$, $q_{1t}, q_{2t} > 10$ GeV	0.57
WW fusion	0.9332
ZZ fusion	0.02641

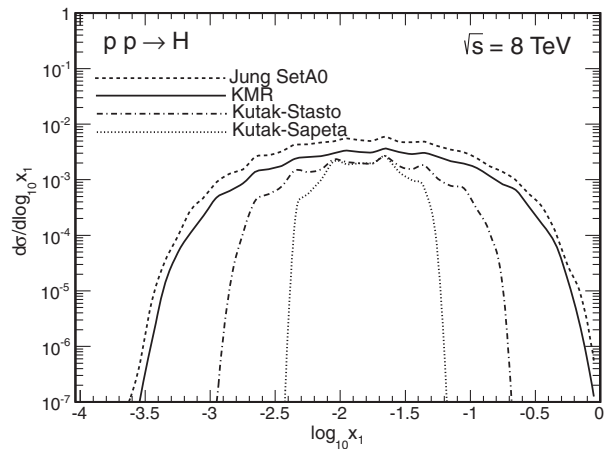


FIG. 6. Distribution in $\log_{10}(x_1)$ or $\log_{10}(x_2)$ for $gg \rightarrow H$ and for different UGDFs used in the present analysis.

In addition, the different UGDFs in the literature have quite different dependence on gluon transverse momenta. This is well demonstrated in Fig. 7 where we show two-dimensional maps in $q_{1t} \times q_{2t}$ for different UGDFs. The Kutak-Sapeta UGDF gives a sharp peak at large q_{1t} and q_{2t} . This means that using such an UGDF one cannot obtain large Higgs boson transverse momenta. Quite large gluon transverse momenta ($q_{1t}, q_{2t} \sim m_H$) enter the production of the Higgs boson for the KMR and Jung CCFM (setA0) UGDFs. For the KMR UGDF a clear enhancement at small q_{1t} or q_{2t} can be observed. This is rather a region of nonperturbative nature, where the KMR UGDF is rather extrapolated than calculated. However, we have checked that the contribution of the region when $q_{1t} < 2$ GeV or $q_{2t} < 2$ GeV constitutes only less than 5% of the integrated cross section. This is then a simple estimate of uncertainty of the whole approach.

Now we can proceed to the production of photons. We start from two-dimensional distributions in $\frac{d\sigma}{dydp_t}$ in rapidity

and transverse momentum of the Higgs boson calculated according to Eq. (2.3) and perform its decay isotropically in the Higgs boson rest frame (assuming spin zero of the Higgs boson). Next relativistic boosts are performed to get distributions of photons in the proton-proton center-of-mass system. As an example in Fig. 8 we show two-dimensional distributions in photon transverse momenta. Also here the distributions for different UGDFs differ significantly. In Fig. 9 we show in addition two examples but in the contour form which shows some details better than the lego plot.

In order to confront our calculations with the preliminary ATLAS data [14] extra cuts on photon rapidities and transverse momenta must be imposed in addition. We require

$$\begin{aligned} -2.37 < \eta_{\gamma,1}, \eta_{\gamma,2} < 2.37, \quad \max(p_{1t}, p_{2t}) > 0.35 \times M_{\gamma\gamma}, \\ \min(p_{1t}, p_{2t}) > 0.25 \times M_{\gamma\gamma}, \quad 105 \text{ GeV} < M_{\gamma\gamma} < 160 \text{ GeV} \end{aligned} \quad (3.1)$$

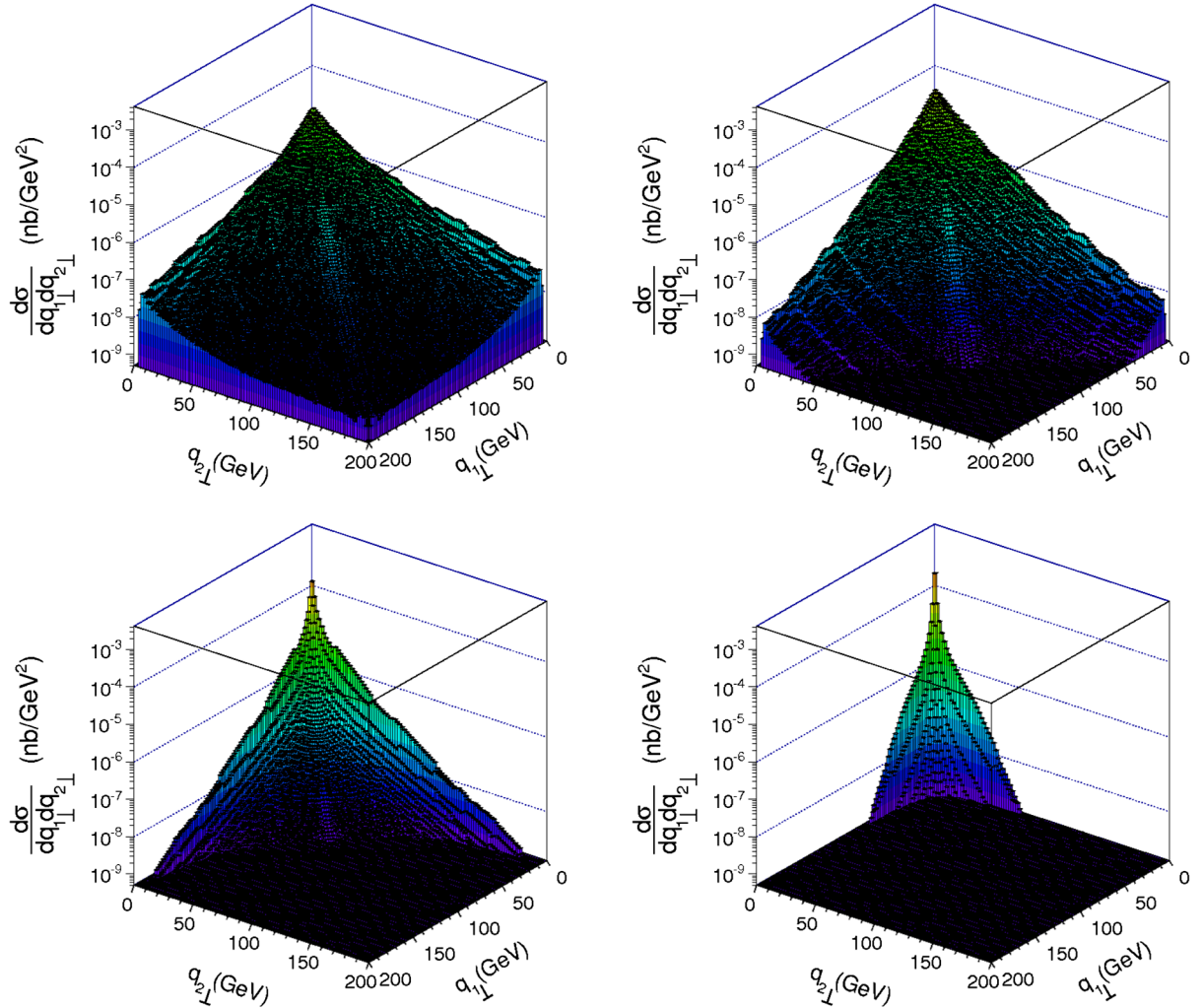


FIG. 7 (color online). Distribution in q_{1t} and q_{2t} for $gg \rightarrow H$ and for different UGDFs: KMR, Jung CCFM (setA0), Kutak-Staśto and Kutak-Sapeta.

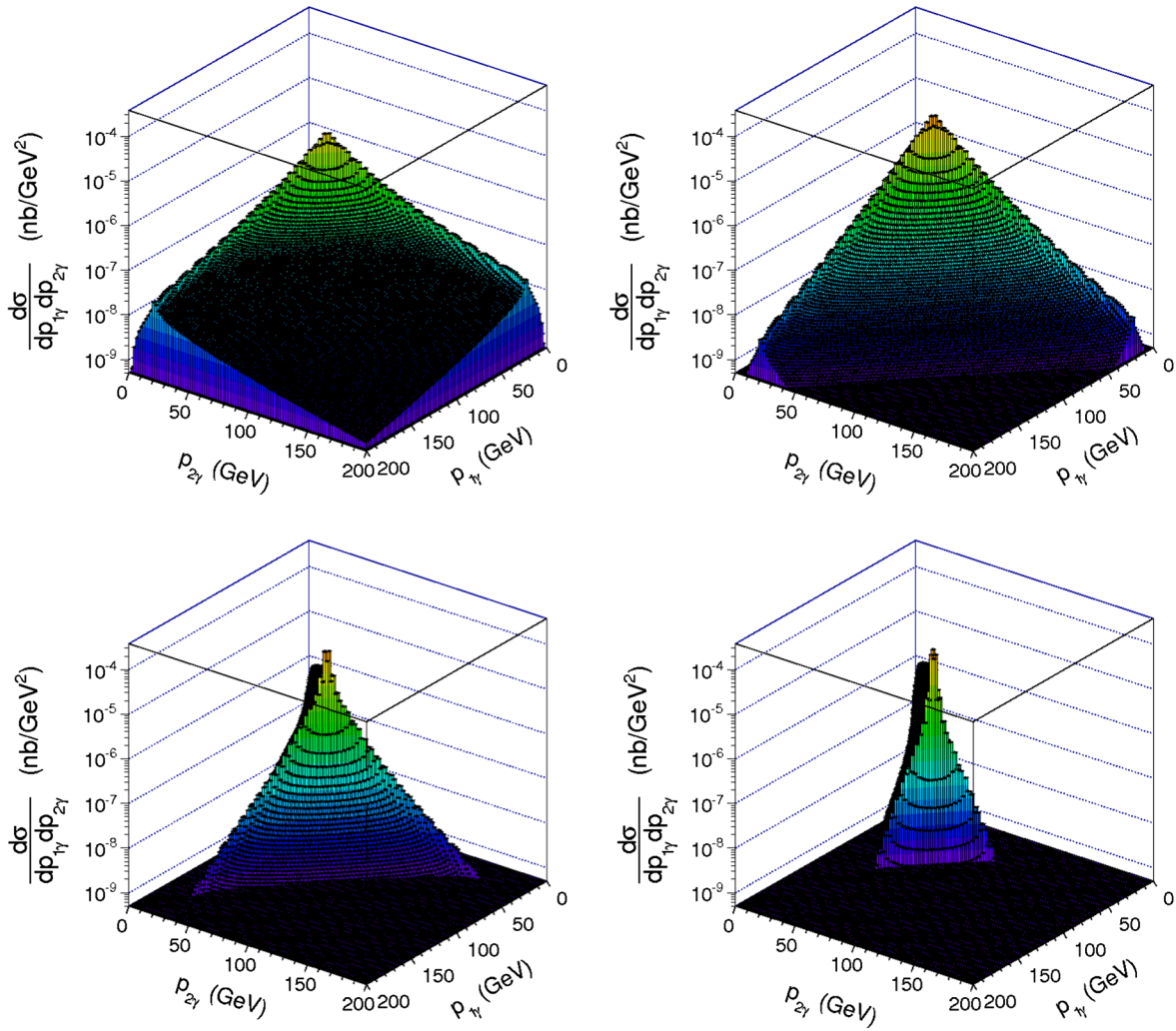


FIG. 8 (color online). Distributions in photon transverse momenta p_{1t} and p_{2t} for the $gg \rightarrow H$ and for the KMR, Jung CCFM (setA0), Kutak-Stasto and Kutak-Sapeta UGDFs.

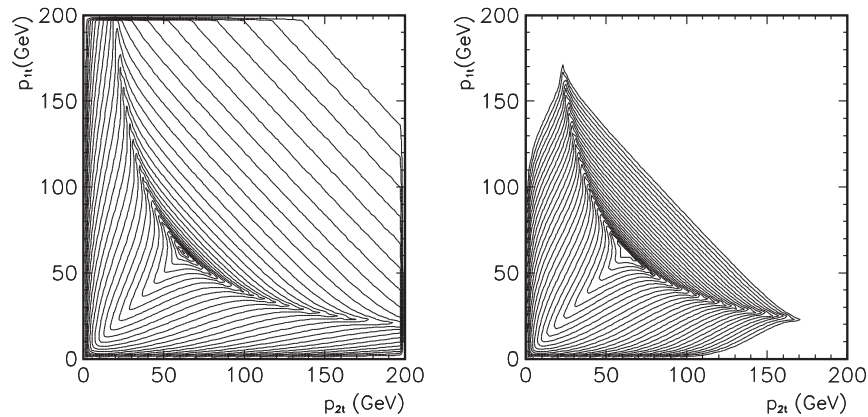


FIG. 9. Distributions in photon transverse momenta p_{1t} and p_{2t} for $gg \rightarrow H$ and for the KMR and Jung CCFM (setA0) UGDFs for the contour representation.

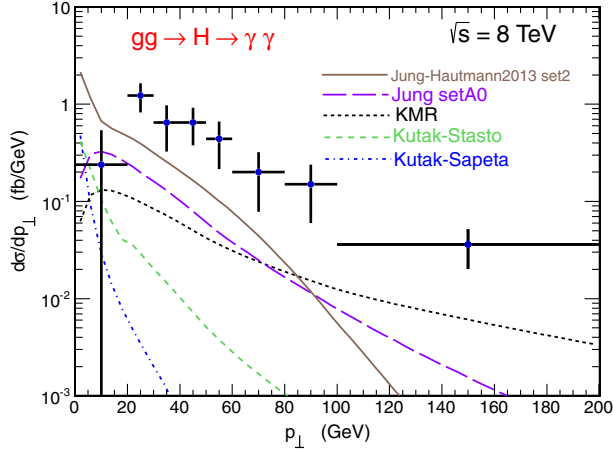


FIG. 10 (color online). Transverse momentum distribution of the Higgs boson produced in the $gg \rightarrow H$ subprocess in the $\gamma\gamma$ channels for different UGDFs from the literature.

as relevant for the ATLAS analysis [14]. The distribution in the transverse momentum of the photon pair (almost transverse momentum of the Higgs boson) is shown in Fig. 10 for different UGDFs from the literature together with the ATLAS data [14]. The calculated distributions lie much below the ATLAS data. How the situation can be improved including Higgs off-shell effects, higher-order QCD and electroweak corrections will be discussed in the rest of the paper.

B. $gg \rightarrow H^* \rightarrow \gamma\gamma$

In this section we shall present the results of calculations performed within the k_t factorization approach in the second method. The photon distributions from virtual Higgs decay are calculated including correctly kinematics of the $2 \rightarrow 2$ subprocess $gg \rightarrow H^* \rightarrow \gamma\gamma$. Now we wish to compare differential cross sections obtained in this way with those obtained within the first method. Clearly the second method leads to sizeably larger cross sections. This may be helpful in the context of the deficit discussed in the previous section, but certainly not sufficient. At this point we observe a disagreement (of about a factor of 2) of the results of our $gg \rightarrow H^* \rightarrow \gamma\gamma$ calculation with those in Ref. [10].

In Fig. 11, as an example, we show a somewhat theoretical distribution in $\log_{10}(x_i)$, $i = 1, 2$ for the KMR UGDF with $\mu^2 = m_H^2$. Both low- x ($x < 10^{-2}$) and high- x ($x > 10^{-2}$) regions give similar contributions to the cross section.

In Fig. 12 we show the distribution in p_{1t} or p_{2t} (identical) for the two methods. The two distributions are rather similar as far as the shape is considered.

The distribution in $p_{t,\text{sum}}$ ($\vec{p}_{t,\text{sum}} = \vec{p}_{1t} + \vec{p}_{2t}$) is particularly interesting as it reflects the distribution of the Higgs boson and can be measured experimentally. In Fig. 13 we again compare the results obtained within the two methods. The shapes obtained with the two methods are practically identical but there is a difference in the normalization.

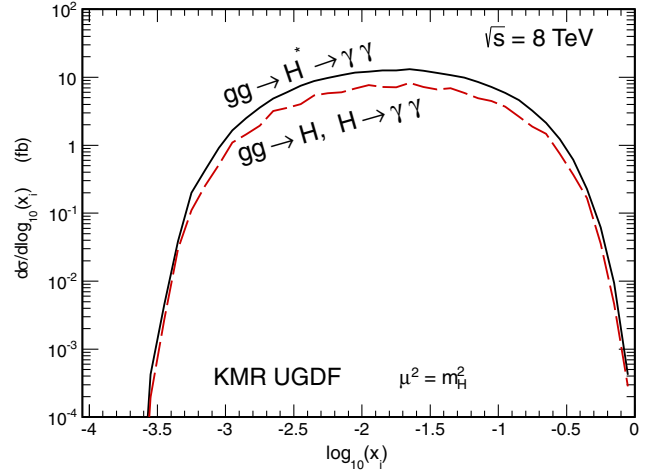


FIG. 11 (color online). Distribution in $\log_{10} x_i$ for the KMR UGDF and $\mu^2 = m_H^2$ for the first (on-shell Higgs boson, long-dashed line) and second (off-shell Higgs boson, solid line) method.

Now we wish to show several results for the second approach only. Let us start from the single-photon transverse momentum distribution. In Fig. 14 we show such distributions for two selected UGDFs. The peak at $p_t \sim m_H/2$ is of kinematical nature. The KMR UGDF leads to larger photon transverse momenta.

Particularly interesting is distribution in the two-photon invariant mass. The huge peak at $M_{\gamma\gamma} = M_H$ corresponds to the on-shell Higgs boson. We observe (see Fig. 15) small contributions from off-shell Higgs boson configurations with invariant masses both smaller or larger than the on-shell (peak) value. The sharp peak shows that the integration of the cross section is not easy. We have, however, carefully checked the convergence.

As was already mentioned, the distribution for $p_{t,\text{sum}}$ reflects the Higgs boson transverse momenta. An interesting

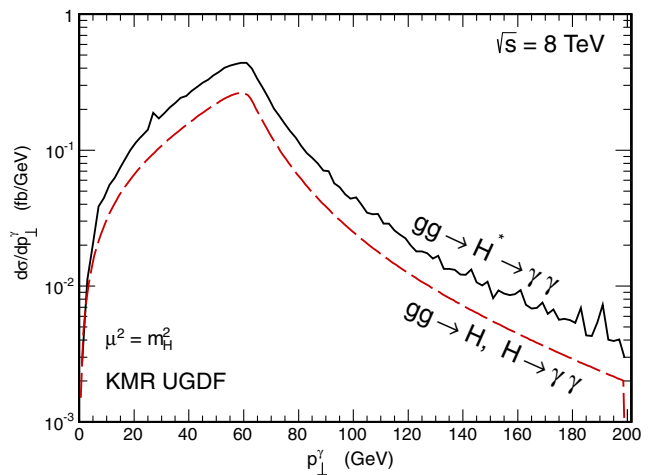


FIG. 12 (color online). Distribution in p_{it} ($i = 1, 2$) for the KMR UGDF and $\mu^2 = m_H^2$ for the first (long-dashed line) and second (solid line) method.

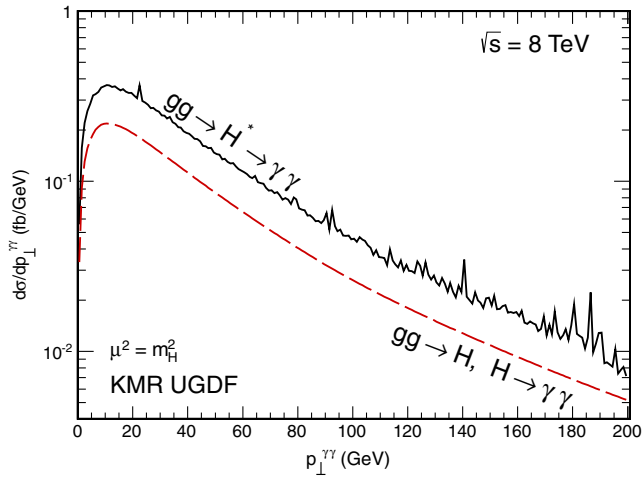


FIG. 13 (color online). Distribution in $p_{t,\text{sum}}$ for the KMR UGDF and $\mu^2 = m_H^2$ for the first (long-dashed line) and second (solid line) method.

question is how the distribution is sensitive to the choice of the UGDF model. Figure 16 shows that the KMR UGDF generates much bigger Higgs boson transverse momenta than the Jung CCFM (setA0).

Another interesting observable is the correlation in the azimuthal angle between the outgoing photons (see Fig. 17). A bigger back-to-back correlation is observed for the Jung CCFM (setA0) than for the KMR UGDF. This is similar as already observed for the azimuthal correlations between $c\bar{c}$ (see e.g. Ref. [41]). The decorrelation for the KMR UGDF is even larger (compare only shapes) than in the soft-gluon transverse momentum resummation [8]. Small $\phi_{\gamma\gamma}$ are strongly correlated with large gluon transverse momenta q_{1t} or q_{2t} . As discussed above this may be overestimated in the k_t -factorization approach with the KMR UGDF.

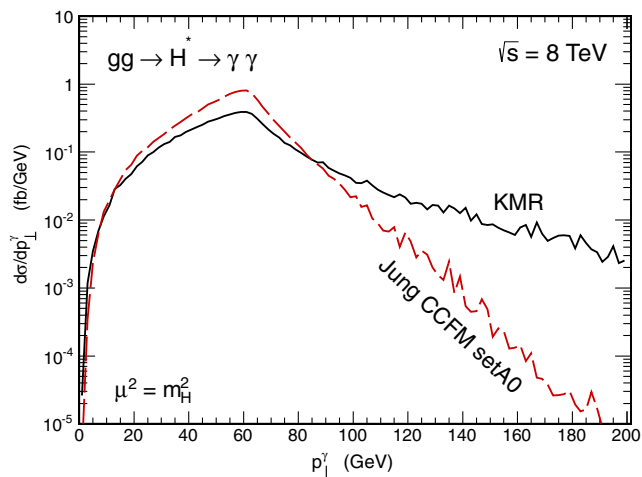


FIG. 14 (color online). Distribution of the photon transverse momentum for the KMR (solid line) and the Jung CCFM (setA0) (long-dashed line) UGDF, for $\mu^2 = m_H^2$.

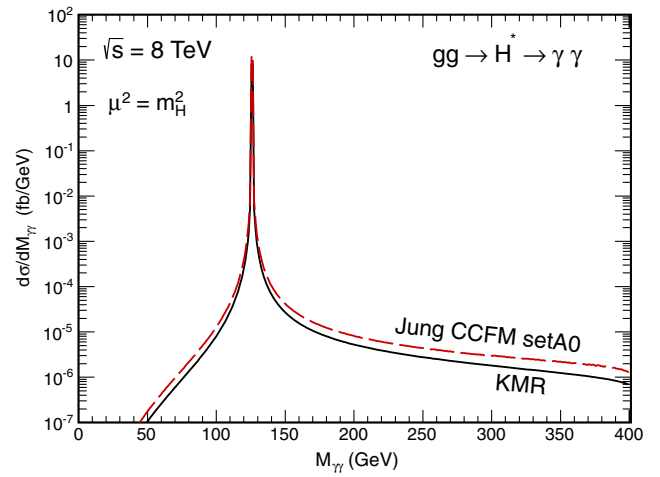


FIG. 15 (color online). Distribution of diphoton invariant mass for the KMR (solid line) and the Jung CCFM (setA0) (long-dashed line) UGDF, for $\mu^2 = m_H^2$.

In Fig. 18 we show rather theoretical distributions in “initial” gluon transverse momenta. Those distributions are almost identical to those discussed already for on-shell Higgs boson production (see Fig. 7). The distribution for the KMR UGDF is broader than that for the Jung CCFM (setA0) UGDF.

Finally we wish to present two-dimensional correlations in photon transverse momenta (see Fig. 19). Again this distribution is similar to its counterpart obtained within the first method (compare Fig. 8).

C. Higgs in association with one jet (gluon)

Now we wish to show some results of the calculation for Higgs + gluon production within the k_t -factorization approach.

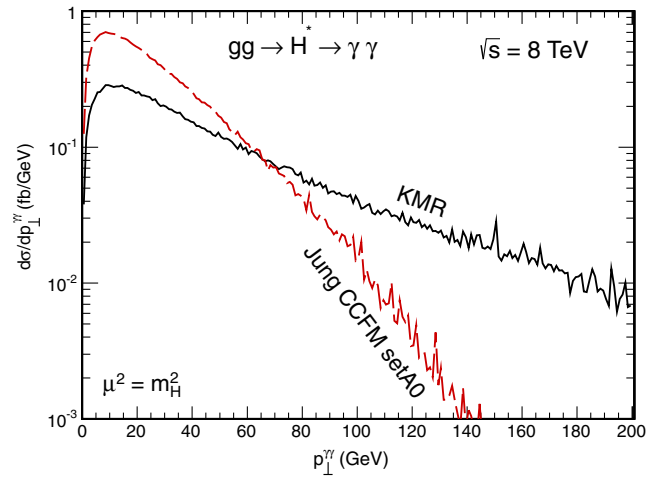


FIG. 16 (color online). Distribution of diphoton transverse momentum for the KMR (solid line) and the Jung CCFM (setA0) (long-dashed line) UGDF, for $\mu^2 = m_H^2$.

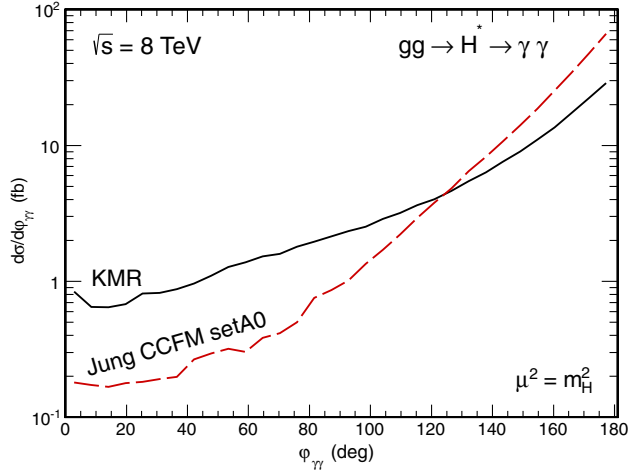


FIG. 17 (color online). Distribution of the azimuthal angle between photons for the KMR (solid line) and the Jung CCFM (setA0) (long-dashed line) UGDF, for $\mu^2 = m_H^2$.

We start from a pedagogical two-dimensional distribution (a similar distribution was discussed in the context of the $gg \rightarrow H$ mechanism) in initial gluon transverse momenta (q_{1t}, q_{2t}). In Fig. 20 we show the distribution for the four different UGDFs used also for the $gg \rightarrow H$ calculation.

The Higgs transverse momentum distribution is particularly interesting in the context of the preliminary ATLAS data. In leading-order collinear approximation the distribution in the Higgs transverse momentum (transverse momentum of the photon-photon pair in our analysis) is a two-dimensional delta function. Nonzero transverse momenta are obtained only in next-to-leading-order approximation. In Fig. 21 we show the result of the collinear NLO calculation. In addition we show the result of our calculation in the k_t factorization with the KMR

UGDFs. One can observe the coincidence of both results at large Higgs transverse momenta. In addition the singularity present in the collinear approach disappears in the k_t -factorization approach.

In Fig. 22 we show distributions in the transverse momentum for all the five UGDFs from the literature used in the present study. It is worth to notice that in all cases the inclusion of gluon transverse momenta automatically removes singular behavior of the cross section at $p_t \rightarrow 0$. We observe that the cross section for $gg \rightarrow Hg$ is of the same order of magnitude as that calculated before for $gg \rightarrow H$. We wish to notice here that in contrast to other gluon-initiated processes the dominant piece of the $gg \rightarrow Hg$ is not included in the calculation of $gg \rightarrow H$. This can be easily understood by inspecting the diagrams in Figs. 1 and 2. While for the $gg \rightarrow H$ fusion the triangle with top quarks is the dominant mechanism, in the case of the $gg \rightarrow Hg$ process these are the diagrams with top-quark boxes that dominate. This can be easily understood already in the collinear next-to-leading-order calculation by switching only the terms corresponding either to triangles or boxes separately (see also a discussion in the early papers on the subject [32]). It can be easily checked that at LHC energies triangles play an important role only at small transverse momenta of the Higgs boson. Above $p_t > 50$ GeV the contribution of the triangles is negligibly small compared to the contribution of the boxes. The same is of course true for the k_t -factorization approach.

Due to their completely different topology the diagrams with boxes are certainly not contained in our previous calculations for the $gg \rightarrow H$ fusion. The same is true for all previous calculations of the Higgs boson production in the k_t factorization [10,20,23,24].

In Fig. 23 we show the sum of the leading ($gg \rightarrow H$) and the next-to-leading ($gg \rightarrow Hg$) contributions again for the

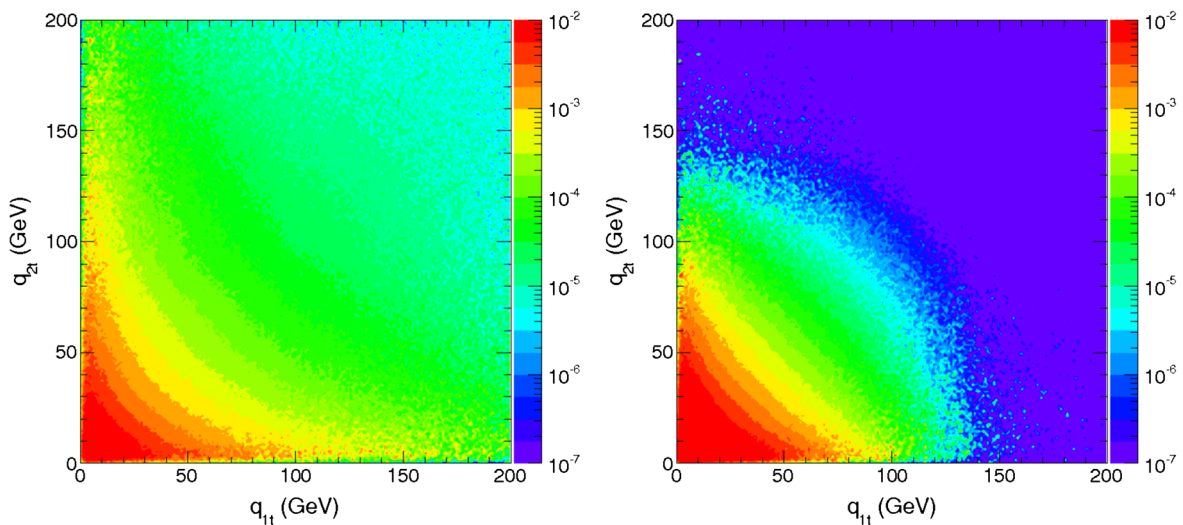


FIG. 18 (color online). Two-dimensional distribution in (q_{1t}, q_{2t}) for the KMR (left panel) and for the Jung CCFM (setA0) (right panel) UGDF and for $\mu^2 = m_H^2$.

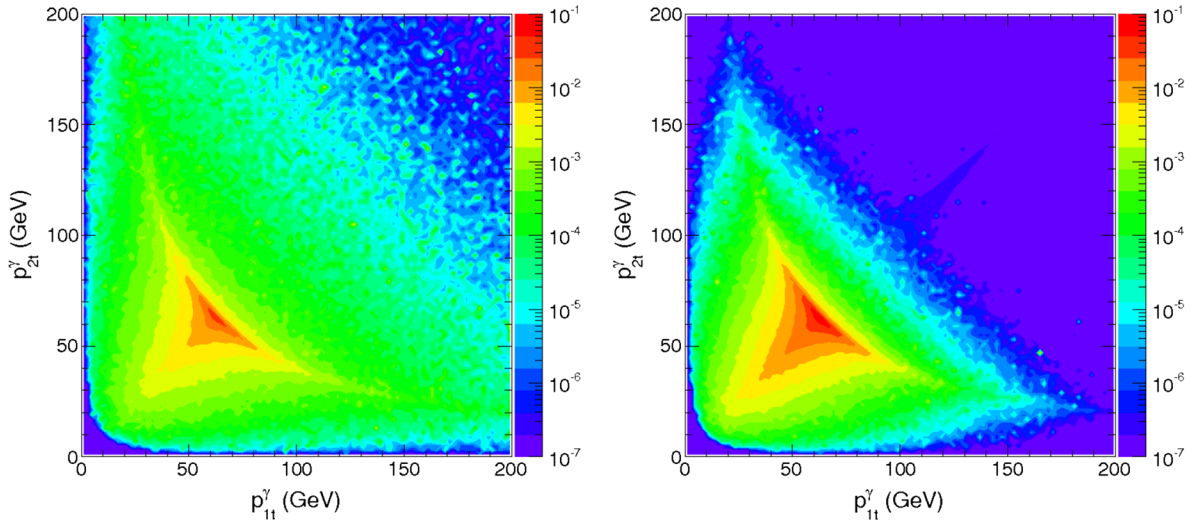


FIG. 19 (color online). Two-dimensional distribution in photon transverse momenta (p_{1t}, p_{2t}) for the KMR (left panel) and for the Jung CCFM (setA0) (right panel) UGDF and for $\mu^2 = m_H^2$.

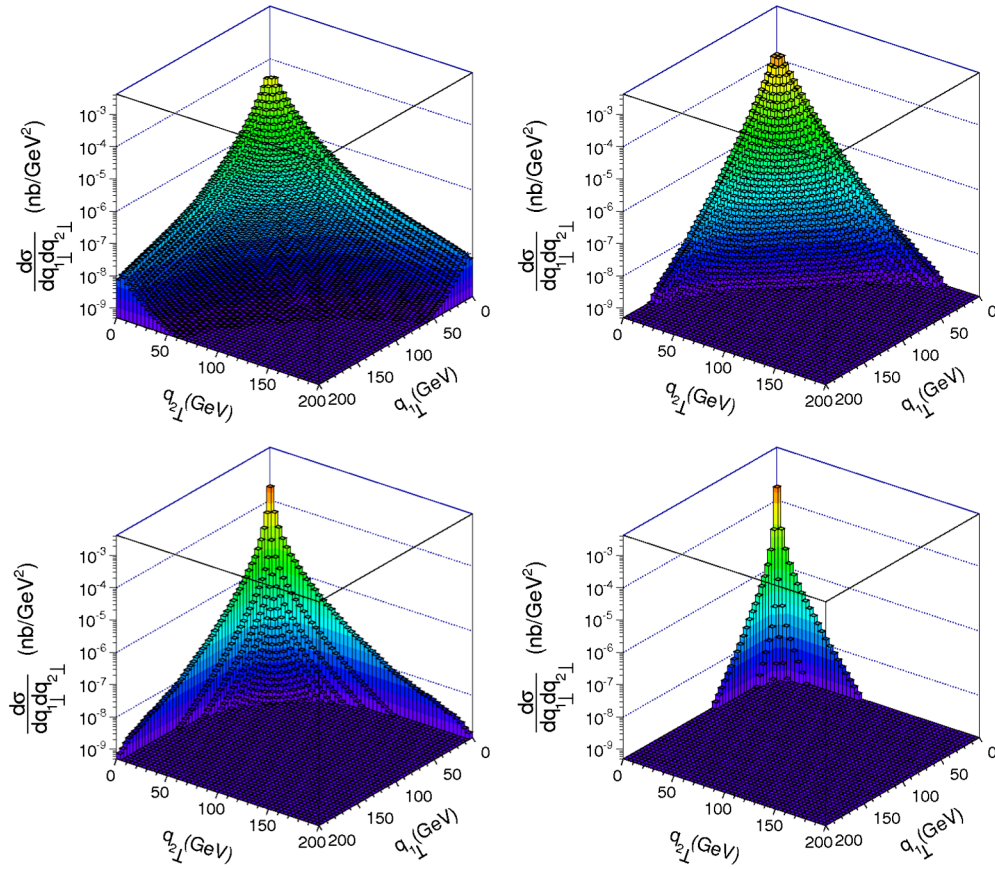


FIG. 20 (color online). Two-dimensional distribution in (q_{1t}, q_{2t}) for the $gg \rightarrow Hg$ process for the four different UGDFs used previously also for the $gg \rightarrow H$ calculation: KMR UGDF and $\mu_F^2 = m_H^2$ (left top panel) and Jung CCFM setA0 (right top panel), Kutak-Stařto (left bottom panel) and Kutak-Sapeta (right bottom panel).

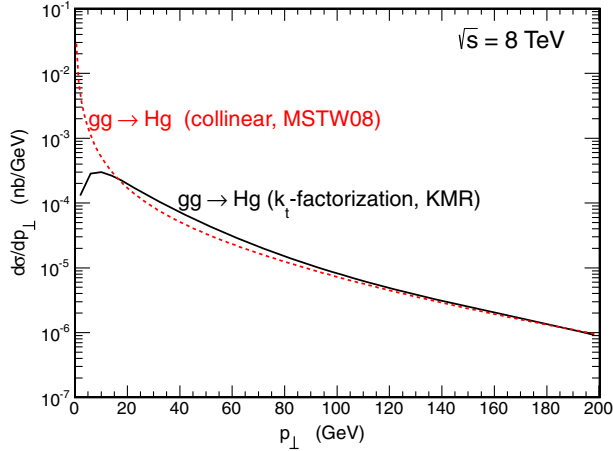


FIG. 21 (color online). Comparison of the standard collinear NLO result (dashed line) with our k_t -factorization result (solid line).

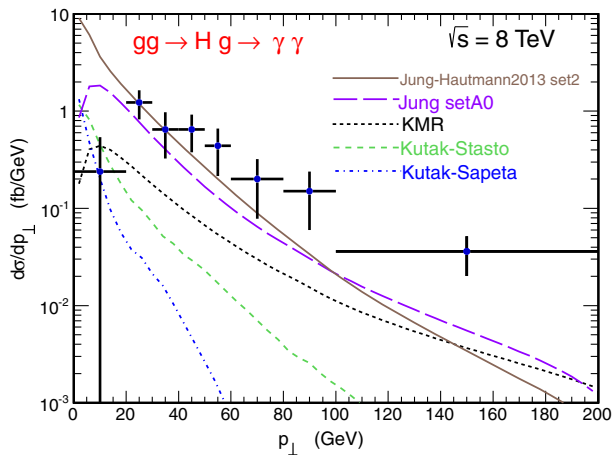


FIG. 22 (color online). Transverse momentum distribution of the Higgs boson in the $\gamma\gamma$ channel produced in the $gg \rightarrow Hg$ subprocess for the different UGDFs from the literature.

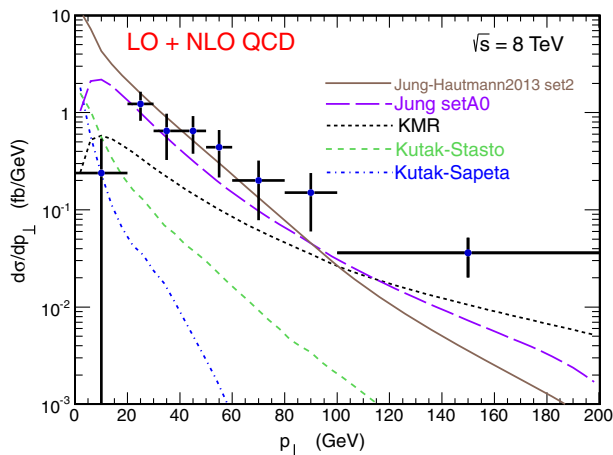


FIG. 23 (color online). Transverse momentum distribution of the Higgs boson in the $\gamma\gamma$ channel produced in the $gg \rightarrow H$ and in the $gg \rightarrow Hg$ subprocesses for the different UGDFs from the literature.

different UGDFs used so far. The result for the KMR and Jung CCFM setA0 UGDFs is already almost consistent with the new ATLAS data. The electroweak contribution will be discussed below.

D. Higgs in association of two jets

It is interesting to compare the k_t -factorization calculation at large q_{1t} and q_{2t} (transverse momenta of the fusing gluons) with the standard (collinear) calculation of the Higgs boson production associated with two jets. In Fig. 24 we show a two-dimensional distribution in the space of the transverse momenta of the associated jets (p_{3t}, p_{4t}) for the $gg \rightarrow gHg$ process only. Since the initial gluons are collinear this is also exactly the distribution in (q_{1t}, q_{2t}) (transverse momenta of the t -channel gluons) and can be directly compared with similar distributions obtained previously in the k_t -factorization $gg \rightarrow H$ calculation. In this calculation the high-energy limit and rapidity ordering (see Ref. [39]) were assumed. The shape here is similar to that for the KMR UGDF. However, the absolute normalization is sizeably smaller. We think that such contributions are therefore effectively included in the calculation with the KMR UGDF. But this is certainly not true for saturation-inspired UGDFs.

The contributions of the $gq(\bar{q})$, $q(\bar{q})$ and $(q(\bar{q}), q(\bar{q}))$ discussed previously in the formalism section are usually not included explicitly in the k_t -factorization approach with most of the UGDFs (except for the KMR UGDF) and has to be taken into account when comparing the theoretical results to the experimental data.

Let us make further comparison of the results for $gg \rightarrow gHg$ with $p_{3t}, p_{4t} < 10$ GeV (which automatically means $q_{1t}, q_{2t} < 10$ GeV) with a similar result obtained within the k_t -factorization approach for $gg \rightarrow H$ with the KMR UGDF. From Table I we see that the result for the KMR UGDF is much bigger than that for the $gg \rightarrow gHg$ collinear-factorization approach. This is difficult to understand as in the KMR model the whole transverse momentum is generated in the last step of the ladder. In Fig. 25 we show distributions in $\log_{10}(x_1)$ or $\log_{10}(x_2)$ for both cases. One clearly sees that the x 's for the k_t -factorization approach [maximum at $\log_{10}(x_i) \approx -1$] are smaller than their counterparts for the $gg \rightarrow gHg$ [maximum at $\log_{10}(x_i) \approx -2$]. This explains the huge cross section at large q_{1t} and/or large q_{2t} within the k_t -factorization approach for $gg \rightarrow H$ which does not include fully correctly the kinematics of the actual process (missing jets are not included in calculating x_1 and x_2). It is not clear to us how to consistently correct the calculation for the kinematical effect.

E. Other contributions

In Fig. 26 we compare contributions of different mechanisms. The QCD contributions shown in this subsection were calculated with the KMR UGDF. Surprisingly the

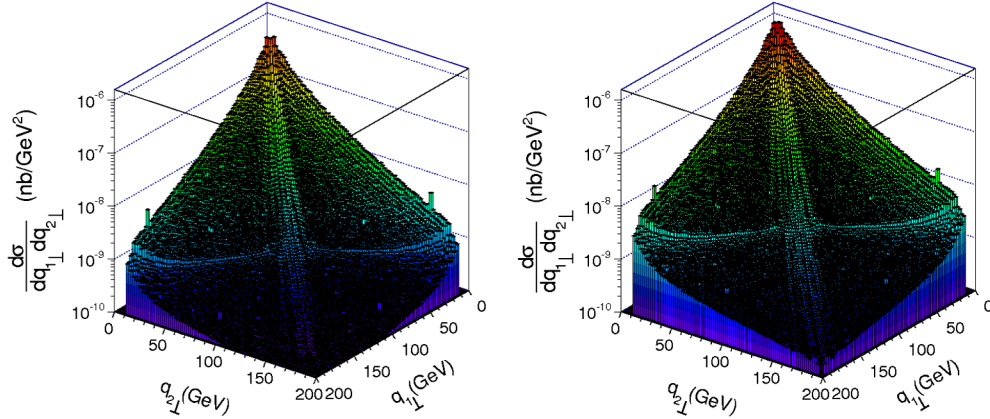


FIG. 24 (color online). Two-dimensional distribution in jet transverse momenta (p_{3t}, p_{4t}) for the $2 \rightarrow 3$ process $gg \rightarrow gHg$ (left) and $ij \rightarrow iHj$ (right). In this calculation $\mu_F^2 = m_H^2$ and $\mu_{r,1}^2 = p_{3t}^2, \mu_{r,2}^2 = p_{4t}^2$. A cut on $p_{3t}, p_{4t} > 10$ GeV has been assumed in addition.

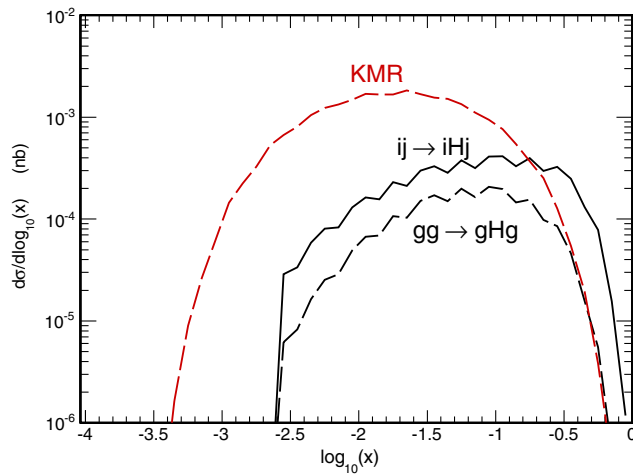


FIG. 25 (color online). $\log_{10}(x_i)$ distribution for the k_t -factorization approach for $gg \rightarrow H$ (upper dashed line, red online) and for $gg \rightarrow gHg$ (lower dashed line) and $ij \rightarrow iHj$ (solid line) for $q_{1t}, q_{2t} > 10$ GeV.

contribution of the next-to-leading-order mechanism $gg \rightarrow Hg$ is even slightly bigger than that for the $gg \rightarrow H$ fusion, especially for intermediate Higgs boson transverse momenta. As already discussed, there is almost no double counting when adding the corresponding cross sections due to quite different Feynman diagram topology. As shown in the present analysis the $gg \rightarrow H$ mechanism is not sufficient within the k_t -factorization approach. The $2 \rightarrow 3$ contribution of the $gg \rightarrow gHg$ subprocess is probably also quite large but here one can expect that a big part is already contained in the $gg \rightarrow H$ calculation especially with the KMR UGDF. Therefore we do not add this contribution explicitly when calculating $d\sigma/dp_{t,\text{sum}}$. The contribution of the WW, ZZ fusion is also fairly sizeable. In principle, the Higgs bosons (or photons from the Higgs boson) could be to some extent isolated by requiring a rapidity gap i.e. the production of the Higgs boson isolated off other hadronic activity.

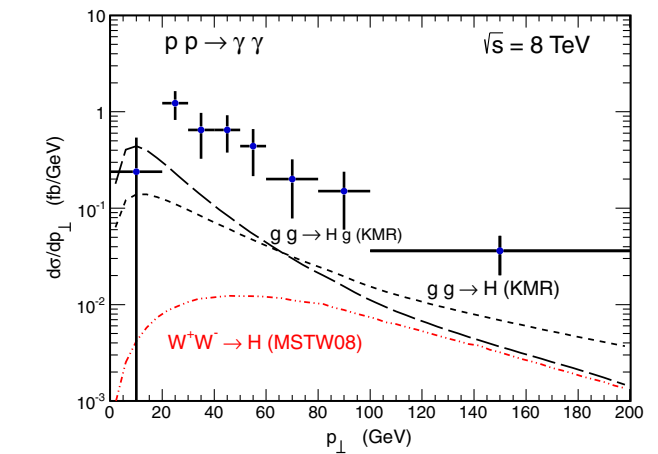


FIG. 26 (color online). Transverse momentum distribution of the Higgs boson in the $\gamma\gamma$ channels for different mechanisms: $gg \rightarrow H$ (solid line), $gg \rightarrow Hg$ (dashed line) and $WW \rightarrow H$ (dash-dotted line).

If we added the contribution together we would almost describe the ATLAS data.

In the future one could include into such an analysis an even higher-order $gg \rightarrow gHg$ contribution as well as associated production $gg \rightarrow tH\bar{t}, q\bar{q} \rightarrow WH$ and $q\bar{q} \rightarrow ZH$. Their contributions are known to be only slightly smaller than the contribution of the WW and ZZ fusion.

IV. CONCLUSIONS

In the light of new ATLAS data we have carefully analyzed Higgs boson production in the $\gamma\gamma$ channel. We have concentrated rather on QCD contributions. The $gg \rightarrow H$ mechanism has been considered within the k_t -factorization approach. Different unintegrated gluon distributions from the literature have been used. In general, the cross section for the leading-order Higgs production within the k_t -factorization approach is somewhat smaller than its counterpart for the leading-order collinear approximation.

We have calculated the cross section for $gg \rightarrow H \rightarrow \gamma\gamma$ within two methods. In the first method we have performed decay of the on-shell Higgs boson within a Monte Carlo method using the $H \rightarrow \gamma\gamma$ branching fraction known from the literature. In the second method we have performed direct calculation with an explicit $2 \rightarrow 2$ $gg \rightarrow H^* \rightarrow \gamma\gamma$ subprocess. In the second method the intermediate Higgs boson is off-mass-shell. The two methods give slightly different results. We have carefully discussed the corresponding differences. The second, more proper method leads to a small enhancement of the cross section with respect to the first method. If this is the explanation of the enhancement of the $\gamma\gamma$ channel as observed by the ATLAS and CMS collaborations requires further studies.

In contrast to recent claims in the literature, the leading-order $gg \rightarrow H$ calculation does not describe the preliminary ATLAS data when correct Standard Model couplings are taken into account. Higher-order corrections within k_t factorization such as $gg \rightarrow Hg$ have been discussed in addition. Their contribution turned out to be of similar order as that for $gg \rightarrow H$. We have argued that there is almost no double counting when adding the leading-order $gg \rightarrow H$ and next-to-leading-order $gg \rightarrow Hg$ contributions in the k_t -factorization approach. The reason is that the box diagrams dominate for the $gg \rightarrow Hg$ subprocess and they are not present in the leading-order $gg \rightarrow H$ subprocess. Also $ij \rightarrow iHj$ ($i, j = q, \bar{q}g$) collinear NNLO contributions have been shown to be rather sizeable, also those with

quarks and/or antiquarks that are certainly not included in the leading-order k_t -factorization approach.

In addition, we have calculated purely electroweak contributions of the WW and ZZ fusion and associated production $qq' \rightarrow WH$ and $qq \rightarrow ZH$. In general, the electroweak contributions are also not negligible.

The sum of all (QCD and electroweak) contributions gives a result which is almost consistent with the ATLAS preliminary data. This requires, however, a further analysis as some double counting between the leading-order ($gg \rightarrow H$), next-to-leading-order ($gg \rightarrow Hg$) and NNLO ($gg \rightarrow gHg$) contributions have to be carefully studied in this approach.

In summary, the production of the Higgs boson in the $\gamma\gamma$ channel can be used to test unintegrated gluon distributions provided all contributions to the cross section are carefully taken into account.

ACKNOWLEDGMENTS

We are indebted to Simone Marzani for information about some references related to our work and Nikolai Zotov for pointing out a misprint in our first manuscript on arXiv. We are also indebted to the authors of Ref. [10] for explaining some details of their calculation after the first version of our paper was submitted. This work was partially supported by the Polish Narodowe Centrum Nauki (NCN) Grants No. DEC-2011/01/B/ST2/04535 and No. DEC-2013/09/D/ST2/03724.

-
- [1] ATLAS Collaboration, *Phys. Lett. B* **716**, 1 (2012); S. Chatrchyan *et al.* (CMS Collaboration), *Phys. Lett. B* **716**, 30 (2012).
- [2] ATLAS Collaboration, *Phys. Lett. B* **726**, 88 (2013); **734**, 406(E) (2014).
- [3] S. Chatrchyan *et al.* (CMS Collaboration), *Phys. Rev. D* **89**, 092007 (2014).
- [4] V. Khachatryan *et al.* (CMS Collaboration), *Phys. Lett. B* **736**, 64 (2014).
- [5] ATLAS Collaboration, *Phys. Rev. D* **90**, 052004 (2014).
- [6] R. V. Harlander and W. B. Kilgore, *Phys. Rev. Lett.* **88**, 201801 (2002); C. Anastasiou and K. Melnikov, *Nucl. Phys.* **B646**, 220 (2002); V. Ravindran, J. Smith, and W. L. van Neerven, *Nucl. Phys.* **B665**, 325 (2003).
- [7] D. de Florian, G. Ferrera, M. Grazzini, and D. Tommasini, *J. High Energy Phys.* **11** (2011) 064.
- [8] D. de Florian, G. Ferrera, M. Grazzini, and D. Tommasini, *J. High Energy Phys.* **06** (2012) 132.
- [9] P. Cipriano, S. Dooling, A. Grebenyuk, P. Gunnellini, F. Hautmann, H. Jung, and P. Katsas, *Phys. Rev. D* **88**, 097501 (2013).
- [10] A. V. Lipatov, M. A. Malyshev, and N. P. Zotov, *Phys. Lett. B* **735**, 79 (2014); arXiv:1402.6481.
- [11] M. A. Kimber, A. D. Martin, and M. G. Ryskin, *Phys. Rev. D* **63**, 114027 (2001); G. Watt, A. D. Martin, and M. G. Ryskin, *Eur. Phys. J. C* **31**, 73 (2003).
- [12] H. Jung and G. P. Salam, *Eur. Phys. J. C* **19**, 351 (2001); H. Jung, arXiv:hep-ph/0411287.
- [13] F. Hautmann and H. Jung, *Nucl. Phys.* **B883**, 1 (2014).
- [14] ATLAS Collaboration, Report No. ATLAS-CONF-2013-072, 2013.
- [15] K. Kutak and A. M. Staśto, *Eur. Phys. J. C* **41**, 343 (2005).
- [16] K. Kutak and S. Sapeta, *Phys. Rev. D* **86**, 094043 (2012); arXiv:1205.5035.
- [17] S. Catani, M. Ciafaloni, and F. Hautmann, *Phys. Lett. B* **242**, 97 (1990); *Nucl. Phys.* **B366**, 135 (1991).
- [18] J. C. Collins and R. K. Ellis, *Nucl. Phys.* **B360**, 3 (1991).
- [19] R. K. Ellis, W. J. Stirling, and B. R. Webber, *QCD and Collider Physics* (Cambridge University Press, Cambridge, England, 2003).
- [20] M. Łuszczak and A. Szczurek, *Eur. Phys. J. C* **46**, 123 (2006).
- [21] F. Hautmann, *Phys. Lett. B* **535**, 159 (2002).
- [22] J. Kwieciński and A. Szczurek, *Nucl. Phys.* **B680**, 164 (2004).
- [23] A. V. Lipatov and N. P. Zotov, *Eur. Phys. J. C* **44**, 559 (2005).

- [24] R. S. Pasechnik, O. V. Teryaev, and A. Szczurek, *Eur. Phys. J. C* **47**, 429 (2006).
- [25] S. Marzani, R. D. Ball, V. Del Duca, S. Forte, and A. Vicini, *Nucl. Phys.* **B800**, 127 (2008).
- [26] V. D. Barger and R. J. N. Phillips, *Front. Phys.* **71**, 592 (1987).
- [27] A. Denner, S. Heinemeyer, I. Puljak, D. Rebuszi, and M. Spira, *Eur. Phys. J. C* **71**, 1753 (2011); [arXiv:1107.5909](https://arxiv.org/abs/1107.5909).
- [28] A. Djouadi, J. Kalinowski, and M. Spira, *Comput. Phys. Commun.* **108**, 56 (1998).
- [29] Y. Liao and X. Li, *Phys. Lett. B* **396**, 225 (1997).
- [30] M. Łuszczak and A. Szczurek, *Phys. Rev. D* **73**, 054028 (2006).
- [31] G. P. Lepage, *J. Comput. Phys.* **27**, 192 (1978).
- [32] R. K. Ellis, I. Hinchliffe, M. Soldate, and J. J. van der Bij, *Nucl. Phys.* **B297**, 221 (1988); U. Baur and E. W. N. Glover, *Nucl. Phys.* **B339**, 38 (1990).
- [33] T. Figy, D. Zeppenfeld, and C. Oleari, *Phys. Rev. D* **68**, 073005 (2003).
- [34] R. N. Cahn and S. Dawson, *Phys. Lett.* **136B**, 196 (1984).
- [35] M. Ciccolini, A. Denner, and S. Dittmaier, *Phys. Rev. D* **77**, 013002 (2008).
- [36] P. Bolzoni, F. Maltoni, S.-O. Moch, and M. Zaro, *Phys. Rev. D* **85**, 035002 (2012).
- [37] S. L. Glashow, D. V. Nanopoulos, and A. Yildiz, *Phys. Rev. D* **18**, 1724 (1978).
- [38] V. Del Duca, W. Kilgore, C. Oleari, C. Schmidt, and D. Zeppenfeld, *Phys. Rev. Lett.* **87**, 122001 (2001); *Nucl. Phys.* **B616**, 367 (2001).
- [39] V. Del Duca, W. Kilgore, C. Oleari, C. R. Schmidt, and D. Zeppenfeld, *Phys. Rev. D* **67**, 073003 (2003).
- [40] V. Barone and E. Predazzi, *High-Energy Particle Diffraction* (Springer, Berlin, 2002).
- [41] R. Maciuła and A. Szczurek, *Phys. Rev. D* **87**, 094022 (2013).